Journal of Structural Biology 176 (2011) 302–306

Contents lists available at SciVerse ScienceDirect

Journal of Structural Biology

journal homepage: www.elsevier.com/locate/yjsbi

# A quantitative collagen fibers orientation assessment using birefringence measurements: Calibration and application to human osteons

Ewa M. Spiesz [a,*], Werner Kaminsky [b], Philippe K. Zysset [a]

[a] Institute of Lightweight Design and Structural Biomechanics, Vienna University of Technology, Austria Gusshausstrasse 27-29, A-1040 Vienna, Austria
[b] Department of Chemistry, University of Washington, Seattle, WA 98195, USA

ARTICLE INFO

*Article history:*
Received 16 June 2011
Received in revised form 14 September 2011
Accepted 20 September 2011
Available online 28 September 2011

*Keywords:*
Collagen fibers orientation
Polarized light
Bone
Mineralized turkey leg tendon

ABSTRACT

Even though mechanical properties depend strongly on the arrangement of collagen fibers in mineralized tissues, it is not yet well resolved. Only a few semi-quantitative evaluations of the fiber arrangement in bone, like spectroscopic techniques or circularly polarized light microscopy methods are available. In this study the out-of-plane collagen arrangement angle was calibrated to the linear birefringence of a longitudinally fibered mineralized turkey leg tendon cut at variety of angles to the main axis. The calibration curve was applied to human cortical bone osteons to quantify the out-of-plane collagen fibers arrangement. The proposed calibration curve is normalized to sample thickness and wavelength of the probing light to enable a universally applicable quantitative assessment. This approach may improve our understanding of the fibrillar structure of bone and its implications on mechanical properties.



## 1. Introduction

Composites with fibers reinforcement are a very frequent motives in the design of natural materials (Fratzl and Weinkamer, 2007). A complex design is required as fibers are usually strong in tension, but rather weak in compression, as they tend to buckle easily. Tissue mineralization is widely used as a predictor of mechanical performance of mineralized tissues, but as the correlation between the mineral content and stiffness measured for example with nanoindentation technique is rather moderate (Boivin et al., 2008; Follet et al., 2004; Zebaze et al., 2011), the attempts of including other factors like morphology of the organic matrix are gaining attention (Siegmund et al., 2008; Willems et al., 2011). Not only volume fraction of organic matter (Reisinger et al., 2010), but also spatial arrangements are of interest for understanding the exceptional elastic properties of bone. The question of how the mineralized collagen fibers are arranged in the extracellular matrix of bone was investigated for over a century, but there is no full agreement on its details. A first model of arrangement of collagen in lamellae was proposed by Gebhard in 1906. The model assumed an unidirectional arrangement of the fibers with an abrupt change of 90° between neighboring lamellae. The next model by Ascenzi and Bonucci (1967, 1968) assumed osteons with mainly longitudinal, transverse or alternating fibril orientation. More recent works present a view that the arrangement of fibers in a lamella follows a certain orientation pattern. The most popular models are the orthogonal plywood pattern similar to the model of Gebhard and that of twisted plywood, characterized by a continuous fibril rotation. A more refined model was proposed by Weiner et al. (1997, 1999), where a single lamella is divided into five sublayers with consecutive rotation of the fibers of 30°. A simulation study by Reisinger et al. (2011) showed that different collagen orientation patterns lead to different elastic properties and anisotropy of a lamella. The models fitting the experimental nanoindentation results best were those by Weiner (Weiner et al., 1999; Wagermaier et al., 2006).

Some methods of direct measurement of collagen out-of-plane orientation (the angle that collagen fibers make with the normal to the specimen surface) are available, like for example scanning small angle X-ray scattering (SAXS) and wide angle X-ray diffraction (WAXD) (Wagermaier et al., 2006). Polarized light measurements were applied to assess the collagen arrangement, but not in a fully quantitative way by Martin and Ishida (1989), Boyde and Riggs (1990), Hengsberger et al. (2002), Bromage et al. (2003) and Skedros et al. (2009), even though birefringence measurement techniques are frequently used as a standard tool in studying anisotropic properties of materials for nearly 200 years (Pajdzik and Glazer, 2006).

Quantitative birefringence assessment requires additional components for the optical set-up (like optical retarders, for the full filters arrangement see Kaminsky et al. (2007)). Some methods allow quantitative measurements of two dimensional linear birefringence (Geday et al., 2000). An addition of a sample tilting stage provides three dimensional maps of birefringence and eigen rays (Pajdzik

* Corresponding author. Fax: +43 1 588 01 31799.
*E-mail address:* ewa.spiesz@ilsb.tuwien.ac.at (E.M. Spiesz).

1047-8477/$ - see front matter © 2011 Elsevier Inc. All rights reserved.
doi:10.1016/j.jsb.2011.09.009

and Glazer, 2006). Recently, a technique allowing a simultaneous imaging of birefringence from four quadrants of a single image at camera speed was developed by Kaminsky et al. (2007). This method, previously applied to some examples from the fields of biology and materials sciences, was here calibrated for the use on mineralized tissues (mineralized turkey leg tendon – MTLT and osteonal bone).

In previous implementations of polarized light methods, the assumption was made that osteons appear completely bright or dark when they are composed of mostly transversely or longitudinally oriented fibers (Boyde and Riggs, 1990; Martin et al., 1996). In between, a brightness ratio was used as indicator of the fraction of longitudinal versus transverse fibers in a sample (Boyde and Riggs, 1990; Ramasamy and Akkus, 2007). This allowed for a comparative evaluation of collagen arrangement in distinct parts of bone (Kalmey and Lovejoy, 2002; Goldman et al., 2003), but did not provide fully quantitative information on the out-of-plane collagen arrangement angle. Additionally the thickness of samples used in the studies was not included in transformation of the birefringence information to the preferred collagen arrangement angle and therefore had to be normalized (Boyde and Riggs, 1990). Alternatively a scale describing six secondary osteons morphotypes was proposed by Martin et al. (1996) and than updated by Skedros et al. (2009). The scale describes different osteons types based on birefringence patterns and assigns scores to each. Averaging over large fields of view results in an average score that is correlated to the average collagen arrangement in a bone section. No quantitative data on the actual out-of-plane collagen angle is provided, but the trends describing mostly transversely or mostly longitudinally arranged fibers are well represented.

As the anisotropy of bone structure reflects its organization, some acoustic microscopy studies could provide information about bone ultrastructure. Turner et al. (1995) measured the average out-of-plane collagen angle of 30° in demineralized osteonal bone.

Some attempts of understanding the arrangement of collagen fibers in osteons was made using Raman microspectroscopic imaging (Kazanci et al., 2006, 2007; Gamsjaeger et al., 2010) providing insight into the organization of bone at the ultrastructural level. This technique requires critical data analysis due to a dependency of the mineral to matrix ratios on materials composition and/or orientation. Measurements of $\nu_1PO_4$/amide I ratios as a function of light polarization angle showed trends that are promising for evaluation of collagen arrangement in bone (Gamsjaeger et al., 2010).

Another method of evaluation of collagen alignment in mineralized tissues is the second harmonic generation microscopy (SHG) that utilizes nonlinear scattering of photons from collagen fibers. Maps trends of collagen being aligned more within or transverse to the measurement plane are created (Cox et al., 2003; Burket et al., 2011), but no quantitative information is available.

In this study we extended the idea of calibration of the circularly polarized light microscopy technique on an uniaxial mineralized collagenous tissue previously proposed by Bromage et al. (2003). To achieve quantitative information about the birefringence, a model tissue of mineralized turkey leg tendon containing longitudinally arranged mineralized collagen fibers was cut at five angles with respect to its main axis and imaged with polarized light. A calibration curve, taking into account sample thickness, wavelength of the light and non-linear relationship of birefringence and out-of-plane fiber angle, was proposed based on the readings on MTLT. The calibration curve was than used on human femur secondary osteons.

## 2. Methods

### 2.1. Samples

MTLT was used as a model for calibration of the birefringence. This tissue is composed of mineralized collagen fibers – similar in constitution to bone, but with much simpler, uniform arrangement, approximately parallel to the main axis of the tendon. MTLT shows two different morphologies, one highly mineralized and very porous and one with low porosity, densely packed collagen fibers and mineralization similar to that of human cortex. The phase more similar to bone in composition and morphology was chosen for the calibration purposes, as the volume fraction of collagen fibrils, as well as, nanoporosity might affect the observed birefringence (Bromage et al., 2003).

For the calibration, 35 fully mineralized MTLT samples were embedded in epoxy resin. Each sample was cut at five different angles to the tendons main axis 0, 30, 45, 60 and 90 (±5)° (Fig. 1) and mounted to glass slides to obtain an uniform section thickness. All sections were polished to the thickness of approximately 30–60 (±5) μm and thickness was recorded with a microscope with a calibrated precision stage in the $z$ direction. Normalization of the readings for sample thickness was necessary to make the calibration universally applicable, while other investigators had to ensure an uniform sample thicknesses in order to make inter-specimen comparisons (Bromage et al., 2003).

Additionally, thin slices of seven mid-shaft human femur samples were prepared with the same protocol as the MTLT samples. Birefringence was measured in about 200 regions of interest. The obtained calibration curve was applied to transform the $|\sin(\delta)|$ readings into the out of plane collagen angle. The collagen arrangement in about 300 osteons was quantitatively assessed.

### 2.2. Birefringence measurements

An automated technique was applied, based on the rotating polarizer method to unfold quantitatively birefringence, eigenmodes and absorption, where an object is simultaneously imaged at four different polarizer angles in a single image implementing an image multiplexer (Quadview, MAG Biosystems) (Kaminsky et al., 2007). In this way the noise contributions coming from camera drifts, fluctuations of light source and mechanical instabilities of the optical system set-up are minimized (Kaminsky et al., 2007). The system used consisted of a microscope for polarized light, interference filter and broadband quarter-wave retarder to produce incident circular polarized light, as well as the image multiplexer and a CCD camera. Background correction was performed to ensure uniform illumination of the whole field of view in the microscope. The image multiplexer used here contained four polarizers placed at 0°, 45°, 90°, 135° with respect to a horizontal reference, allowing the incident circularly polarized light to go through a sample to the four polarizers simultaneously. The birefringence is measured as a sinusoidal function:

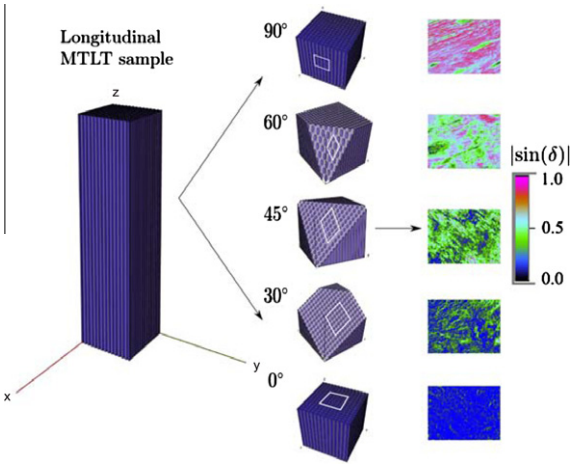


**Fig. 1.** Samples extraction scheme and the resulting $|\sin(\delta)|$ false-colored images.

$$\Delta n_s \approx (n_e - n_o)\sin^2\theta, \tag{1}$$

where $\Delta n_s$ is the birefringence, $n_e$ and $n_o$ are the refractive indices in the direction of extraordinary and ordinary rays, respectively, and $\theta$ is the angle which the wave normal **s** makes with the $z$-axis, which is related to the MTLT fibers and defines the out-of-plane angle of the $z$-axis (see Appendix for the derivation of the formula).

The phase difference $\delta$ between the two light paths (two rays traveling with different velocities – subject to different refractive indices $n_o, n_e$), after the recombination of the rays is a measure of the optical anisotropy of the material (Pajdzik and Glazer, 2006). The phase difference is given by:

$$\delta = \frac{2\pi\Delta n_s L}{\lambda}, \tag{2}$$

with $L$ – sample thickness, $\lambda$ – wavelength of the light. Replacing $\Delta n_s$ with Eq. (16) we obtain:

$$\delta = \frac{2\pi(n_e - n_o)L}{\lambda}\sin^2\theta. \tag{3}$$

In the false colored images the red pixel readings correlate linearly to $|\sin(\delta)|$ . The two morphology zones of MTLT were segmented based on the intensity images. The zone more similar to cortical bone was used for the calibration purposes quantifying the average birefringence of this zone within each image. Pores were also segmented based on the intensity images (Goldman et al., 2003). The fringe-order of the sinusoidal function in Eq. (3) is ambiguous (unless relatively low birefringence is observed), but can be resolved with multiwavelength measurement (Geday et al., 2000). In this study measurements of the $|\sin(\delta)|$ were performed at 550 and 600 nm and the ambiguity elimination procedure described in Geday et al. (2000) was applied.

Solving Eq. (3) for the angle which the wave normal **s** makes with the optical axis $\theta$ introduced into the uniaxial MTLT samples by special angled cuts (see Fig. 1) leads to:

$$\theta = \arcsin\sqrt{c\frac{\delta}{L}}, \tag{4}$$

with the calibration factor $c$:

$$c = \frac{L}{\delta}\sin^2\theta = \frac{\lambda}{2\pi(n_e - n_o)}. \tag{5}$$

## 3. Results

Mean values of thickness normalized $|\sin(\delta)|$ readings were calculated for each region of interest in an acquired image. The ambiguity in the phase measurements was solved using two wavelength measurements. Pixels showing $|\sin(\delta)|$ from other than the first fringe were discarded in the calibration procedure (Pajdzik and Glazer, 2006). The calibration factor $c$ was determined from Eq. (5) to 0.038. The resulting calibration curve is shown in Fig. 2.

### 3.1. Application to human midshaft osteons

The dependency between $|\sin(\delta)|$ and out-of-plane collagen arrangement angle $\theta$ calibrated on MTLT was applied in osteonal bone (see Fig. 3).

The average out-of-plane collagen angle measured on the midshaft sections of human femurs was 25.8° with standard deviation of 1.3°.

Exemplary results are shown in Fig. 3. Different types of osteons were visible, for example osteons with frequently changing collagen arrangement angle between adjacent lamellae (Fig. 3a), called the distributed osteons by Martin et al. (1996). On the other hand, in some osteons the changes were not so frequent (Fig. 3d), with

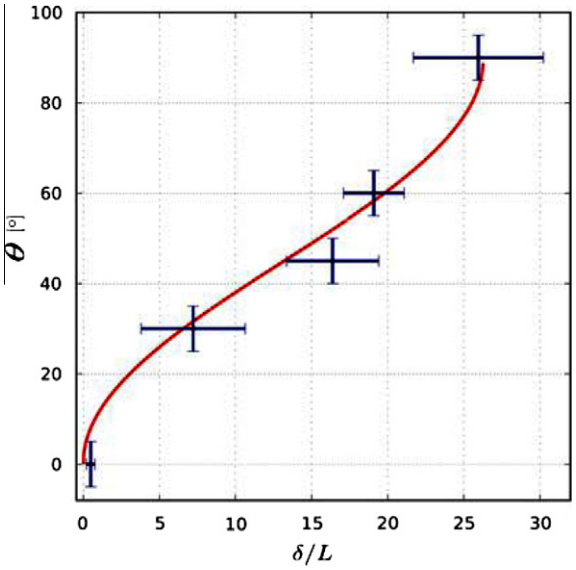


**Fig. 2.** Calibration curve describing relationship between the collagen out-of-plane fibers angle $\theta$ and the measured phase factor $\delta$. Error bars in the $\delta/L$ represent one standard deviation. Sample cut angles $\theta$ were accurate within about 5°.

groups of a few lamellae arranged in similar directions next to a few with another one (called hoop osteons in Martin's scale). Some osteons showed very little changes in collagen arrangement (Fig. 3b), alternatively dark osteons.

An additionally altered collagen arrangement was observed in vicinity of osteocytes (Fig. 3b), exhibiting more of the circumferential type of tissue (Fig. 3c), where the collagen fibers, showing higher birefringence, were arranged longitudinally.

## 4. Discussion

In this study a technique allowing for quantitative assessment of birefringence was calibrated for universal use in mineralized tissues. We believe this is a promising attempt for quantification of collagen fiber arrangement in cortical bone, which is a curtail parameter in many models and can improve our general understanding of the principles underlying the exceptional mechanical properties of bone.

The average collagen orientation observed on seven samples of human femur was about 26°, which is in good agreement with the observations made by Turner et al. (1995) from acoustic micros-

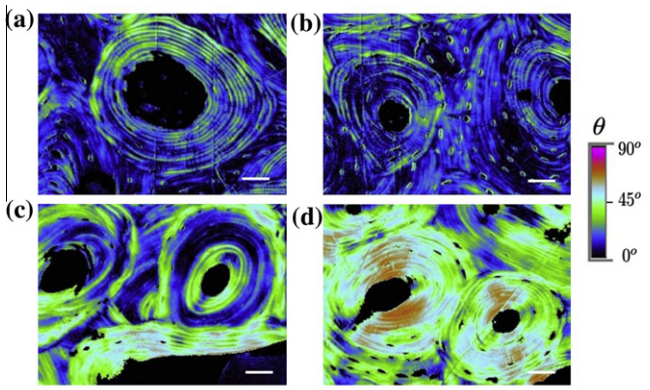


**Fig. 3.** Collagen out-of-plane angles $\theta$ evaluated using the calibration curve on a mid-shaft of human femur. Bar 100 μm.

copy showing a "principal orientation" of collagen at ~30° to the long axis of bone. The acoustic microscope used for the study allowed for a depth resolution of 60 μm. The output of the quantitative light microscopy technique we are introducing here gives the average over the sample thickness seen in transmission at sample thickness of 30–60 μm (resolution in the z direction) which allows for a direct comparison to the acoustic microscopic study, but is in general a limitation of the spatial resolution that can be obtained with the technique. Additionally the study by Turner et al. (1995) showed a misalignment of mineral (that was on average oriented along the long axis of bone) and collagen. The result was interpreted as the contribution of the extrafibrillar mineral, as the interfibrillar mineral is rather well aligned with the collagen fibrils (Gupta et al., 2005; Olszta et al., 2007; Balooch et al., 2008).

According to Weiner et al. (1999) each lamella is composed of five sublayers with collagen fibers rotating progressively about 30° in each. For the sublayers thicknesses presented in that work, the maximum stiffness of such a lamella was predicted in the direction of 12.6° out of plane by Reisinger et al. (2011). Osteons containing lamellae with a similar average collagen arrangement were observed frequently (example in Fig. 3b).Wagermaier et al. (2006) resolved a local crystallite orientation of several osteons of human midshaft femur using scanning X-ray diffraction with a micron-sized synchrotron beam (SAXS/WAXD). The variation of the out-of-plane arrangement of mineral crystallites was 10–60° to the osteon axis and was decreasing with the distance from the Haversian channel. If the arrangement of collagen fibers is assumed to be compliant with the arrangement of the *c* axis of the mineral platelets (Gupta et al., 2005), this could be compared to our results, with the caveat of a potential dependency on the mineral distribution between collagen fibrils and extrafibrillar matrix, as mentioned above (Turner et al., 1995). The average orientation measured with the X-ray diffraction was 30°, similar to what was measured by Turner (Turner et al., 1995) and our results. Wagermaier et al. suggested a 3D helicoidal arrangement of the fibrils around the Haversial channel, since the angles measured were varying within one quadrant. The main advantage of such structures is their higher extensibility in tension and compression, compared to an orthogonal plywood structures (Wagermaier et al., 2006). Anisotropy of a structure with this arrangement is in agreement with the anisotropy predicted by Reisinger et al. (2011) to be about 1.13 (±0.07) for an osteon composed as described by Wagermaier et al. (2006). This fits reasonably to the measured ratio of 1.25 (±0.18) (Franzoso and Zysset, 2009), supporting the helicoidal structure hypothesis in its mechanical implications.

The advantage of using the technique proposed here, over for example SAXS/WAXS techniques, is the possibility of obtaining quantitative information about the collagen fibers arrangement of relatively large regions of the tissue in short experiment time. The limitations of the technique are: the need of thin samples preparation (and control of the thickness) and the fact that volume fraction of the tissue and its degree of mineralization might influence the results. Multiwavelength measurements are required to resolve periodicity ambiguity of the $|\sin(\delta)|$ function. Additionally, slight artifacts were observed in some of the osteon images that manifested in asymmetry of the birefringence readings (as for example in Fig. 3d). Because there is no overall preferred direction common to all images we can conclude that the set-up of polarizing components did not introduce any such artifacts but that they are typical for the samples measured and may indicate background effects from the sample preparation which involved polymers. The effect was taken care in the data analysis by averaging over many samples.

As a validation of the accuracy of the collagen arrangement measurements, spectroscopic (IR and Raman) studies on the angled MTLT samples are planned. Our approach could be extended to other (bio-)materials with birefringent fibers. Further investigations of the collagen out-of-plane angle dependent on physiological location, age, gender and other factors are planned on secondary and primary osteons, as well as, on trabecular bone. Additionally, a combination of the out-of-plane collagen arrangement with the in-plane arrangement assessment that can be as well resolved with polarized light is planned.

## Acknowledgments

This research was supported by Grant No. P19009-N20 of the Austrian Science Foundation (FWF). The authors thank Andreas Reisinger for programing the fibril visualization script used for producing Fig. 1 and Thomas Tangl for help with samples preparation.

## Appendix. Derivation of the calibration formula

The propagation of energy in crystals is described in detail in for example Born and Wolf (1999). The theory of optical anisotropy will be shortly sketched in this section. In a crystal, the energy density $U$ of a wave front is expressed in terms of the electric field $\mathbf{E}$ of the wave and the dielectric displacement $\mathbf{D} = \varepsilon\mathbf{E}$:

$$\mathrm{U} = \frac{1}{2}\mathbf{E}\cdot\mathbf{D}, \tag{6}$$

where the dielectric tensor $\varepsilon$ is of second rank and can be diagonalized. When choosing the orthogonal eigenvectors of $\varepsilon$ as reference, with eigenvalues $\varepsilon_x, \varepsilon_y, \varepsilon_z$ and denoting with $\varepsilon$ the effective dielectric constant with which the light wave propagates along unit vector $\mathbf{s}$ through the sample, than Eq. (6) can be written as:

$$\frac{D^2}{\varepsilon} = 2\mathrm{U} = \frac{D_x^2}{\varepsilon_x} + \frac{D_y^2}{\varepsilon_y} + \frac{D_z^2}{\varepsilon_z}. \tag{7}$$

With $\mathrm{D}^2 = D^2(s_x^2 + s_y^2 + s_z^2)$ follows

$$\frac{s_x^2}{\varepsilon - \varepsilon_x} + \frac{s_y^2}{\varepsilon - \varepsilon_y} + \frac{s_z^2}{\varepsilon - \varepsilon_z} = 0. \tag{8}$$

In this study we assume the uniaxial fiber structure of MTLT is also an optically uniaxial crystal with the optic axis in the $z$ direction, so $\varepsilon_x = \varepsilon_y$. Further we take notation: $\varepsilon_x = \varepsilon_y = \varepsilon_o$, $\varepsilon_z = \varepsilon_e$, where suffixes $o$ and $e$ stand for ordinary and extraordinary. With this notation, the Eq. (8) reduces to:

$$(\varepsilon - \varepsilon_o)[(s_x^2 + s_y^2)(\varepsilon - \varepsilon_e) + s_z^2(\varepsilon - \varepsilon_o)] = 0. \tag{9}$$

Let $\theta$ denote the angle which the wave normal $\mathbf{s}$ makes with the $z$-axis, than:

$$s_x^2 + s_y^2 = \sin^2\theta, \tag{10}$$

$$s_z^2 = \cos^2\theta. \tag{11}$$

Substituting $(s_x^2 + s_y^2)$ and $s_z^2$ in Eq. (9) we obtain:

$$(\varepsilon - \varepsilon_o)[(\varepsilon - \varepsilon_e)\sin^2\theta + (\varepsilon - \varepsilon_o)\cos^2\theta] = 0. \tag{12}$$

This equation has two roots defining the two possible effective dielectric constants $\varepsilon'$, $\varepsilon''$ for a given propagation direction to:

$$\begin{cases} \varepsilon' = \varepsilon_o \\ \varepsilon'' = \varepsilon_o^2\cos\theta + \varepsilon_e\sin^2\theta. \end{cases} \tag{13}$$

With the relation $n^2 = \varepsilon$, with $n$ – average refractive index we derive:

$$\varepsilon'' - \varepsilon' = (\varepsilon_e - \varepsilon_o)\sin^2\theta = n''^2 - n'^2. \tag{14}$$

For small quantities of n we could write:

$$n''^2 - n'^2 \approx \frac{1}{2n}(n'' - n'), \quad n_e^2 - n_o^2 \approx \frac{1}{2n}(n_e - n_o), \tag{15}$$

to derive the birefringence $\Delta n_s = (n'' - n')$ approximately as:

$$\Delta n_s \approx (n_e - n_o)\sin^2\theta. \tag{16}$$

## References


Ascenzi, A., Bonucci, E., 1967. The tensile properties of single osteons. The Anatomical Record 158, 375–386.

Ascenzi, A., Bonucci, E., 1968. The compressive properties of single osteons. The Anatomical Record 161, 377–391.

Balooch, M., Habelitz, S., Kinney, J., Marshall, S., Marshall, G., 2008. Mechanical properties of mineralized collagen fibrils as influenced by demineralization. Journal of Structural Biology 162, 404–410.

Boivin, G., Bala, Y., Doublier, A., Farlay, D., Ste-Marie, L.e., 2008. The role of mineralization and organic matrix in the microhardness of bone tissue from controls and osteoporotic patients. Bone 43, 532–538.

Born, M., Wolf, E., 1999. Principles of Optics. Cambridge University Press, Cambridge, UK.

Boyde, A., Riggs, C., 1990. The quantitative study of the orientation of collagen in compact bone slices. Bone 11, 35–39.

Bromage, T.G., Goldman, H.M., McFarlin, S.C., Warshaw, J., Boyde, A., et al., 2003. Circularly polarized light standards for investigations of collagen fiber orientation in bone. The Anatomical Record Part B: The New Anatomist 274, 157–168.

Burket, J., Gourion-Arsiquaud, S., Havill, L.M., Baker, S.P., Boskey, A.L., et al., 2011. Microstructure and nanomechanical properties in osteons relate to tissue and animal age. Journal of Biomechanics 44, 277–284.

Cox, G., Kable, E., Jones, A., Fraser, I., Manconi, F., et al., 2003. 3-Dimensional imaging of collagen using second harmonic generation. Journal of Structural Biology 141, 53–62.

Follet, H., Boivin, G., Rumelhart, C., Meunier, P.J., 2004. The degree of mineralization is a determinant of bone strength: a study on human calcanei. Bone 34, 783–789.

Franzoso, G., Zysset, P.K., 2009. Elastic anisotropy of human cortical bone secondary osteons measured by nanoindentation. Journal of Biomechanical Engineering 131, 021001-1–021001-11.

Fratzl, P., Weinkamer, R., 2007. Nature's hierarchical materials. Progress in Materials Science 52, 1263–1334.

Gamsjaeger, S., Masic, A., Roschger, P., Kazanci, M., Dunlop, J., et al., 2010. Cortical bone composition and orientation as a function of animal and tissue age in mice by raman spectroscopy. Bone 47, 392–399.

Gebhardt, W., 1906. Ueber funktionell wichtige anordnungsweisen der feineren und groeberen bauelemente des wirbeltierknochens. II. Spezieller teil. der bau der haversschen lamellensysteme und seine funktionelle bedeutung. Archiv fuer Entwicklungsmechanik der Organismen 20, 187–322.

Geday, M., Kaminsky, W., Lewis, J., Glazer, A., 2000. Images of absolute retardance l$\delta n$, using the rotating polariser method. Journal of Microscopy 198, 1–9.

Goldman, H.M., Bromage, T.G., Thomas, C.D.L., Clement, J.G., 2003. Preferred collagen fiber orientation in the human mid-shaft femur. The Anatomical Record Part A: Discoveries in Molecular, Cellular, and Evolutionary Biology 272A, 434–445.

Gupta, H., Wagermaier, W., Zickler, G., Raz-BenAroush, D., Funari, S., et al., 2005. Nanoscale deformation mechanisms in bone. Nano Letters 5, 2108–2111.

Hengsberger, S., Boivin, G., Zysset, P.K., 2002. Morphological and mechanical properties of bone structural units: a two-case study. International Journal of the Japan Society of Mechanical Engineers 45, 936–943.

Kalmey, J.K., Lovejoy, C.O., 2002. Collagen fiber orientation in the femoral necks of apes and humans: do their histological structures reflect differences in locomotor loading? Bone 31, 327–332.

Kaminsky, W., Gunn, E., Sours, R., Kahr, B., 2007. Simultaneous false-colour imaging of birefringence, extinction and transmittance at camera speed. Journal of Microscopy 228, 153–164.

Kazanci, M., Roschger, P., Paschalis, E., Klaushofer, K., Fratzl, P., 2006. Bone osteonal tissues by raman spectral mapping: orientation–composition. Journal of Structural Biology 156, 489–496.

Kazanci, M., Wagner, H., Manjubala, N., Gupta, H., Paschalis, E., et al., 2007. Raman imaging of two orthogonal planes within cortical bone. Bone 41, 456–461.

Martin, R., Ishida, J., 1989. The relative effects of collagen fiber orientation, porosity, density, and mineralization on bone strength. Journal of Biomechanics 22, 419–426.

Martin, R., Lau, S., Mathews, P., Gibson, V., Stover, S., 1996. Collagen fiber organization is related to mechanical properties and remodeling in equine bone a comparison of two methods. Journal of Biomechanics 29, 1515–1521.

Olszta, M.J., Cheng, X., Jee, S.S., Kumar, R., Kim, Y.Y., et al., 2007. Bone structure and formation: a new perspective. Materials Science and Engineering: R: Reports 58, 77–116.

Pajdzik, L.A., Glazer, A.M., 2006. Three-dimensional birefringence imaging with a microscope tilting-stage. Uniaxial crystals. Journal of Applied Crystallography 39, 227–326.

Ramasamy, J., Akkus, O., 2007. Local variations in the micromechanical properties of mouse femur: the involvement of collagen fiber orientation and mineralization. Journal of Biomechanics 40, 910–918.

Reisinger, A., Pahr, D., Zysset, P., 2010. Sensitivity analysis and parametric study of elastic properties of an unidirectional mineralized bone fibril-array using mean field methods. Biomechanics and Modeling in Mechanobiology 9, 499–510.

Reisinger, A., Pahr, D., Zysset, P., 2011. Elastic anisotropy of bone lamellae as a function of fibril orientation pattern. Biomechanics and Modeling in Mechanobiology 10, 67–77.

Siegmund, T., Allen, M., Burr, D., 2008. Failure of mineralized collagen fibrils: modeling the role of collagen cross-linking. Journal of Biomechanics 41, 1427–1435.

Skedros, J.G., Mendenhall, S.D., Kiser, C.J., Winet, H., 2009. Interpreting cortical bone adaptation and load history by quantifying osteon morphotypes in circularly polarized light images. Bone 44, 392–403.

Turner, C.H., Chandran, A., Pidaparti, R.M.V., 1995. The anisotropy of osteonal bone and its ultrastructural implications. Bone 17, 85–89.

Wagermaier, W., Gupta, H.S., Gourrier, A., Burghammer, M., Roschger, P., et al., 2006. Spiral twisting of fiber orientation inside bone lamellae. Biointerphases 1, 1–5.

Weiner, S., Arad, T., Sabanay, I., Traub, W., 1997. Rotated plywood structure of primary lamellar bone in the rat: orientations of the collagen fibril arrays. Bone 20, 509–514.

Weiner, S., Traub, W., Wagner, H., 1999. Lamellar bone: structure–function relations. Journal of Structural Biology 126, 241–255.

Willems, N.M., Mulder, L., Bank, R.A., Grnheid, T., den Toonder, J.M., et al., 2011. Determination of the relationship between collagen cross-links and the bone-tissue stiffness in the porcine mandibular condyle. Journal of Biomechanics 44, 1132–1136.

Zebaze, R.M., Jones, A.C., Pandy, M.G., Knackstedt, M.A., Seeman, E., 2011. Differences in the degree of bone tissue mineralization account for little of the differences in tissue elastic properties. Bone 48, 1246–1251.